A Binary Segmentation Approach for Boxing Ribosome Particles in Cryo EM Micrographs

PS Umesh Adiga[1], Ravi Malladi[1], William Baxter[2], Robert M Glaeser[34]

[1]Computing Sciences Division, LBNL, 1, Cyclotron Road, Berkeley, CA94720,
[2]Wadsworth Center, PO Box 509, Albany, New York 12201,
[3]Physical Biosciences Division, LBNL, 1, Cyclotron Road, Berkeley, CA94720 and
[4]Molecular and Cell Biology, University of California, Berkeley, CA94720.

[1] Author for correspondence,
Umesh Adiga, MS 50A-1148, Lawrence Berkeley National Laboratory, 1, Cyclotron Road, Berkeley CA94720, USA. Ph. (+1) 510 4865296, FAX: (+1) 510 4866199, Email: upadiga@lbl.gov

Abstract

Three-dimensional reconstruction of ribosome particles from electron micrographs requires selection of many single-particle images. Roughly 100,000 particles are required to achieve approximately 10 Å resolution. Manual selection of particles, by visual observation of the micrographs on a computer screen, is recognized as a bottleneck in automated single particle reconstruction. This paper describes an efficient approach for automated boxing of ribosome particles in micrographs. Use of a fast, anisotropic non-linear reaction-diffusion method to pre-process micrographs and rank-leveling to enhance the contrast between particles and the background, followed by binary and morphological segmentation constitute the core of this technique. Modifying the shape of the particles to facilitate segmentation of individual particles within clusters and boxing the isolated particles is successfully attempted. Tests on a limited number of micrographs have shown that over 80% success is achieved in automatic particle picking.

Keywords: micrograph, particle, diffusion, segmentation, boxing

1. Introduction

Electron microscopy (EM) techniques comprise a powerful and diverse collection of methods that facilitate visualization of biological structures at a macromolecular level. Electron microscopy covers a range of resolution that spans several orders of magnitude, bridging the gap between crystallography and light microscopy (Sali et al, 2003). The resolution of an image of macromolecular structures depends on the number of electrons applied to the sample, since a trade-off exists between statistical definition and damage to sample (Glaeser, 1971). Micrographs showing projections of macromolecular assemblies must be recorded at very low electron dose to minimize radiation damage, resulting in low image contrast (Henderson, 1995). Overcoming the limitations posed by the low electron exposures that are "safe" requires merging data from images of up to millions of molecules in order to increase the signal-to-noise ratio. The number of macro-molecule images required for a volumetric reconstruction increases significantly with the resolution of the micrograph (Frank, 1996). When images of currently available quality are used, it is believed that at least one million particles are required to reconstruct a protein-molecule with "atomic" resolution (Henderson, 1995; Sali et al, 2003).

For reconstructing the three-dimensional (3-D) shape of a protein molecule, particles from each micrograph are selected either manually, using interactive graphics software or by computer aided semi-automatic methods. Either method becomes a very labor intensive job when the number of particles required becomes very large. Automation of particle selection is hence necessary to prevent this stage from becoming a serious bottle neck in visualization of the structure of a protein molecule. Several approaches to automate particle picking have been proposed which have met with

varying degrees of success (Nicholson and Glaeser, 2001). Among these, particle extraction based on texture features of candidate particles obtained by peak search of the Gaussian smoothed micrograph was proposed by Lata et al (1995). Although this method remains one of the most effective that has been described to date, many false positives still get through and a manual editing of the resulting data is required as a final step.

In this article, we present a methodology based on non-linear preprocessing of micrographs followed by multi-level, region-based thresholding and morphological segmentation. Our objective is not just extraction of single particles but also to segment those single particles which are located rather close to one-another, thus increasing the throughput of the boxing process without increasing erroneous selection of particles.

2. Segmentation of Ribosome Particle Images

Micrographs of ribosome particles lack clarity and definition because of the high level of electron shot noise mentioned above (Glaeser, 1971). The design of computational techniques that can extract particles from the background and from interfering materials in the image is thus essential. Normalization of the micrographs to have approximately the same mean and grey-level distribution for all the micrographs, followed by anisotropic reaction-diffusion and rank-leveling to smooth the background texture and remove the illumination variation, constitute our initial pre-processing steps. Pre-processed micrographs are then thresholded and individual particles and clusters are separated. Particles within clusters are then segmented by a combined erosion-dilation and region growing algorithm. This is followed by a second stage of particle picking and boxing of the segmented particles in the micrograph.

2.1 Normalization

When we digitize the micrographs, the measured optical density (OD) values reflect the electron image intensity at each point on the micrograph. Within a large data set, however, one can expect to have significant variations in the average electron intensity due to variations in specimen thickness from one micrograph to the next, variations in condenser lens setting, different choice of image magnification from one day to the next and other factors.

Generally, the micrograph pixel values are in a narrow range of the possible grey-scale range. It is therefore helpful to "standardize" all micrographs before segmentation, a step that we have chosen to do by a selective histogram stretching. Histogram stretching, generally known as contrast stretching, also tends to make the image visually more distinctive, a fact that has simplified our work during the process of designing pre-processing and segmentation algorithms. Histogram stretching can be briefly described as follows. If $f(x,y)$ is the image function then the histogram stretch is given by

$$g(x,y) = \frac{(K-1)}{\left(\max_n\{f(x,y)\} - \min_n\{f(x,y)\}\right)}\left(f(x,y) - \min_n\{f(x,y)\}\right)$$; where K is the maximum brightness value in the histogram-stretched image (by default $k = 255.0$). This process brings the OD values of the micrograph into the complete grey-scale range. We have observed that standard histogram stretching, as per the above definition, is not very useful in making the image visually more distinctive or in enhancing the contrast, however. To obtain a better result, we stretch only a selected part of the histogram that contains most of the pixels. The *max* and *min* values are defined as the grey-levels where the histogram curve falls to below $1\% + offset$ and $1\% - offset$ of the number of pixels at

the mode point of the histogram on both sides of the peak respectively. For example, Figure 1 shows, a histogram of a micrograph where the curve falls below 1% of the peak at grey-levels 160 and 230. With *offset* = 20, we calculate *max* =250 and *min* =140. Figure 1, shows the histogram of a micrograph before and after stretching.

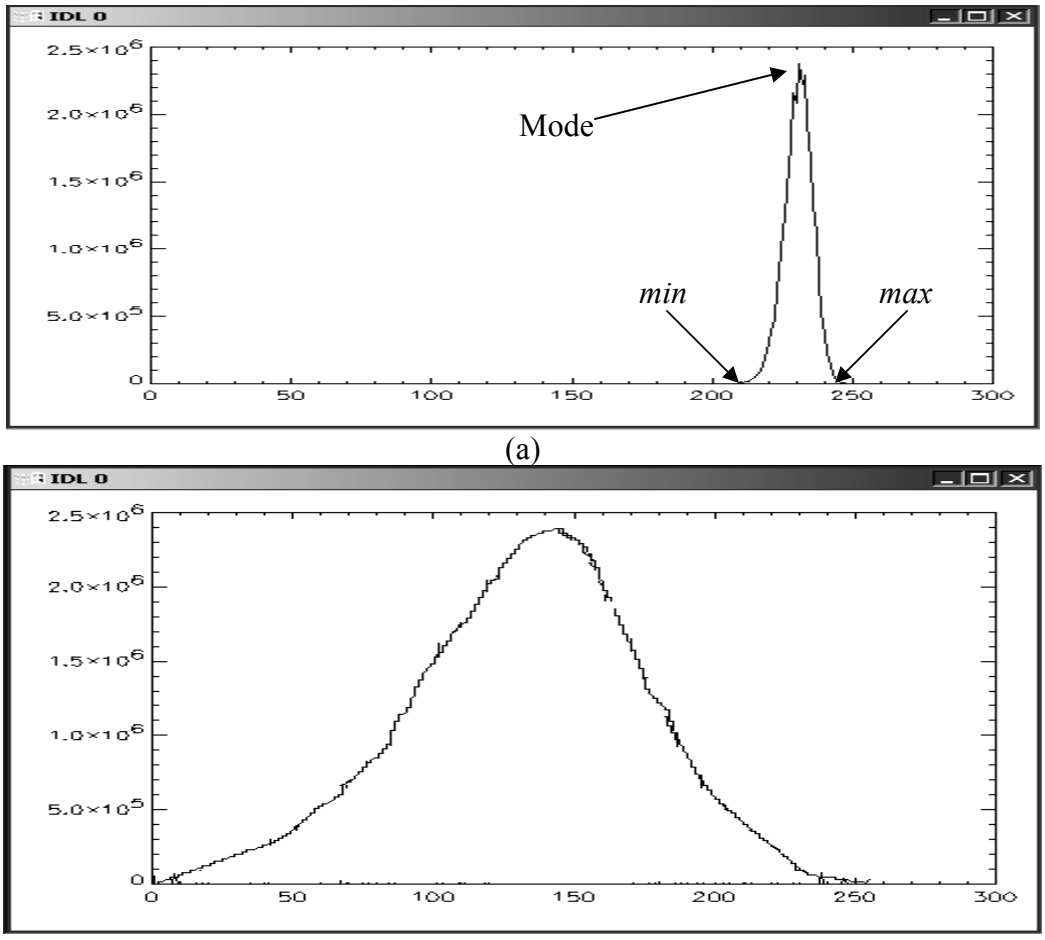

Figure 1: Histogram of a micrograph (a) before (b) after stretching.

Since the *max* and *min* grey-levels calculated, based on the initial histogram curve, are data dependent, the result of histogram stretching standardizes micrographs by tending to produce a common mean and grey-scale distribution. The standardization effect on three micrographs is illustrated in Figure 2.

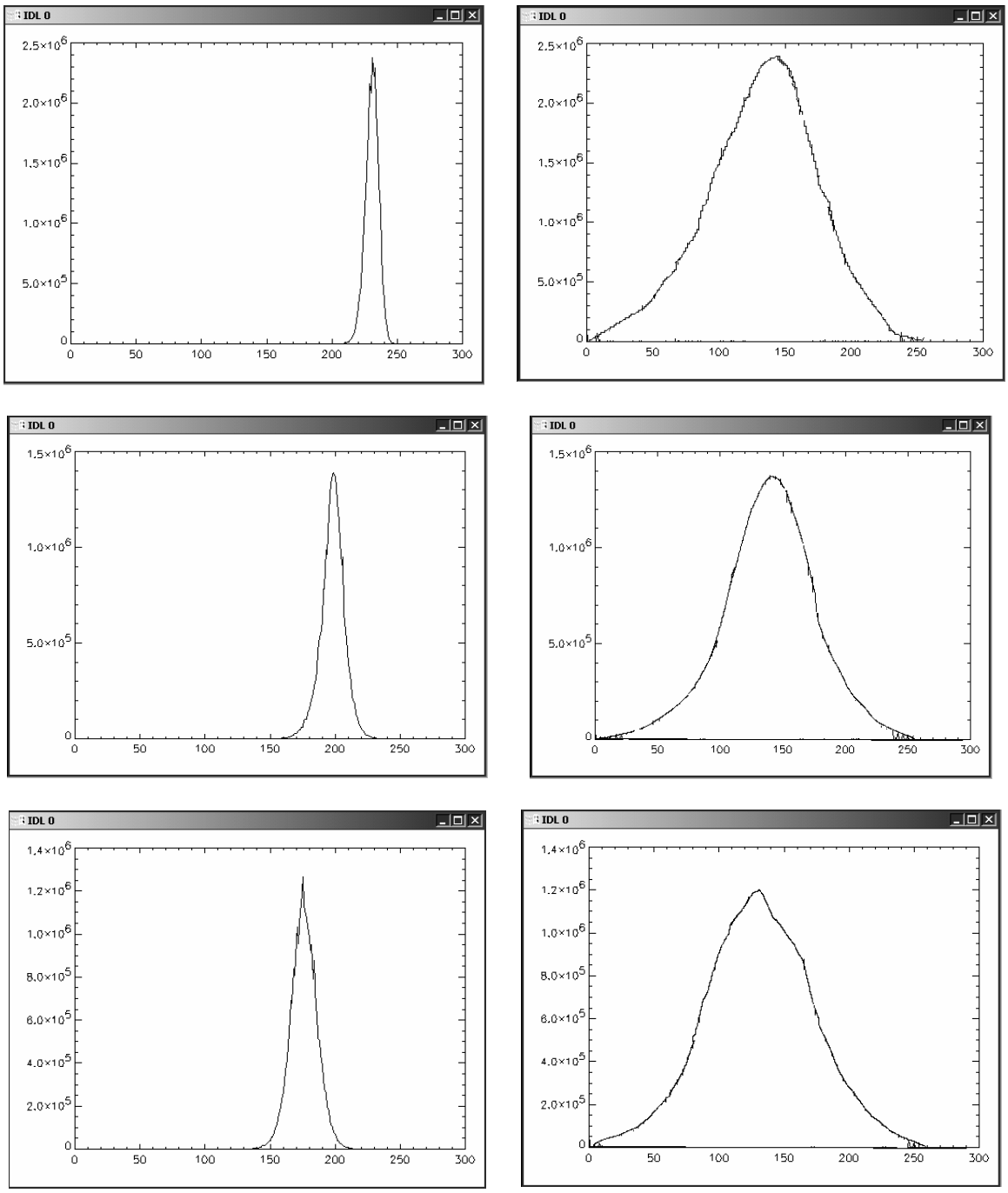

(a) (b)

Figure 2: Illustration of micrograph standardization by selective histogram stretching (a) Original histogram (b) After selective histogram stretching.

2.2 Non-linear Pre-processing

Micrographs, in general, have poor signal to noise ratio (SNR) as has been stated above. The main type of noise that corrupts micrographs of ice embedded specimens is electron shot noise. In order to increase the SNR, a high degree of smoothing of micrographs is required. Smoothing an image using low-pass filters like the Gaussian smoothing filter will also blur the image and compromise the boundary (or the edge) information. What we desire is an image denoising scheme that reduces the background noise and texture variation, while preserving the particle shape boundaries. We employ the non-linear partial differential equation based smoothing technique called the Beltrami flow equation (Sochen et al 1996; 1998).

Consider the image function $U = I(x, y)$. Linear diffusion can be achieved by a parabolic partial differential equation (PDE), namely

$$I_t = \frac{\partial U}{\partial t} = \frac{\partial^2 U}{\partial x^2} + \frac{\partial^2 U}{\partial y^2} \quad . \qquad \text{----- (1)}$$

A discrete equivalent of this equation can be solved with a time step value $\Delta t_{\max} = \frac{1}{2}\left(\frac{1}{\Delta x^2} + \frac{1}{\Delta y^2}\right)^{-1}$, where Δx and Δy denote spatial resolution of the micrographs in x and y dimensions. The linear diffusion given by Eqn.(1) is equivalent to Gaussian smoothing $u(x, y, t) = \left(G_{\sqrt{2t}} * f\right)(x, y)$ for $t > 0$. Here, $G_{\sqrt{2t}}$ is a Gaussian kernel with $\sigma = \sqrt{2t}$ given by $G_{\sqrt{2t}}(x, y) = \frac{1}{2\pi\left(\sqrt{2t}\right)^2} \cdot \exp\left(\frac{|x|^2 + |y|^2}{2\left(\sqrt{2t}\right)^2}\right)$. This process is also called isotropic diffusion. The blurring of important features such as edges that occurs while moving from finer to coarser scales can be avoided by application of anisotropic

diffusion methods. The use of diffusion equation for image processing originated with the work of Perona and Malik (1987) where the authors pre-select a diffusion coefficient that preserves the edge information. A different view on diffusion was achieved by realizing that the iso-intensity contours of the image can be moved under curvature their curvature following the work of Osher and Sethian (1988). Image smoothing by way of level set curvature motion (Alvarez et. al 1992; Rudin et al 1992; Malladi, Sethian 1996), thwarts the diffusion in the edge direction, thereby preserving the edge information.

The main motivation behind the work of Sochen et al. (1996) was to find a natural way of dealing with different types of image mappings, grayscale, color, volumetric etc. The key idea is to view images as embedded maps between two Riemannian manifolds and to define an action potential that provides a measure on the space of these maps. To be specific, let us denote by (Σ,g) the image manifold and its metric, and by (M,h) the image space-feature manifold and its metric, the so-called action potential is the weight of the map X:$\Sigma \rightarrow$M, i.e.

$$S\left[X^i, g_{\mu\nu}, h_{ij}\right] = \int d^m\sigma \sqrt{g} g \partial_\mu X^i \partial_\nu X^j h_{ij}(X), \qquad \text{---------- (2)}$$

where m is the dimension of Σ, g is the determinant of the image metric, $g^{\mu\nu}$ is the inverse of the image metric, and h_{ij} is he metric of the embedding space. This action is the natural generalization of the *L2* norm to non-Euclidean manifolds and is known as the *Polyakov* Action. Minimizing the above potential with respect to the embedding or the feature coordinates leads to different flows that are known in the literature as the Gaussian, curvature flow, etc. We choose a particular minimization, one that sets the first variation of the potential with respect to the embedding to zero. As an example, a gray

level image is an embedding of a surface described as a graph in R^3, as follows: $X:(x,y)\to[x,y,I(x,y)]$ and the metric is defined

$$(g_{ij})=\begin{pmatrix}1+I_x^2 & I_xI_y\\ I_xI_y & 1+I_y^2\end{pmatrix} \qquad \text{--------- (3)}$$

The explicit equation describing the smoothing flow is realized by minimizing the action potential with respect to the third coordinate I, namely

$$I_t=\frac{(1+I_y^2)I_{xx}-2I_xI_yI_{xy}+(1+I_x^2)I_{yy}}{(1+I_x^2+I_y^2)^2}, \qquad \text{--------- (4)}$$

with the initial condition $I(x,y,t=0)=I_0(x,y)$, the noisy image.

The Beltrami flow incorporates the edge indicator function $h=1/(1+I_x^2+I_y^2)$, thus providing a minimum diffusion at the edges and extensive diffusion elsewhere.

Now consider the following reaction-diffusion PDE:

$$\frac{\partial U}{\partial t}=(\cos\beta)\cdot\nabla h\cdot\nabla U+(\sin\beta)\cdot h\cdot\nabla^2U \qquad \text{-------- (5)}$$

This equation is derived by simple algebraic rearrangement of terms in Eqn. (4); see Malladi and Ravve (2001; 2002) for details. The first term, $\{(\cos\beta)\cdot\nabla h\cdot\nabla U\}$ is a reaction term responsible for edge-enhancement while the second term $\{(\sin\beta)\cdot h\cdot\nabla^2U\}$ is a diffusion term responsible for smoothing. β is a parameter that determines the relative contribution of reaction and diffusion terms and varies from 0^o to 90^o. $\beta=0^0$ is a pure reaction term, $\beta=45^0$ is a nonlinear diffusion flow, $\beta=\arctan 2\approx 63.4^0$ is the Beltrami flow (Sochen et al, 1998), and $\beta=90^0$ is the pure diffusion. Thus by suitably selecting β we can achieve desired amount of smoothing without substantially losing

edge information. Implementation and computational details of reaction-diffusion PDE can be obtained from Malladi and Ravve (2002).

Keeping edge information is necessary as it help in accurate marking of boundary of the particles thus, in turn, helps in finding precise shape features and orientation of the particles that are important for 3-D reconstruction. Figure 2 shows the result of smoothing achieved by the reaction-diffusion technique using different values of β, while parameter such as time step for reaction-diffusion are kept same. We have used $\beta = 75^0$. This value is selected experimentally by considering a number of correctly detected particles.

2.3 Background Leveling

Due to variation in the sample thickness and other factors, micrographs normally show some degree of uneven illumination. Such illumination variation could be corrected by removing low frequency components from the image by high-pass filtering or by a least-squares fitting technique. We have used, instead, the rank-leveling approach (Russ, 1995) to remove uneven background illumination and to further reduce the textural nature of the background. The advantage of rank-leveling over least square fitting or low-pass filtering in the frequency domain is that rank-leveling is an adaptive process.

Rank leveling is a multi-step morphological filtering process. In the first step, a background image is constructed by replacing every pixel by the minimum grey level in its neighborhood (if the particles are brighter than the background) until the objects in the image disappear. The neighborhood size is selected based on the approximate size of the object i.e. the particle size in the micrograph. If the objects are darker i.e. have lower grey

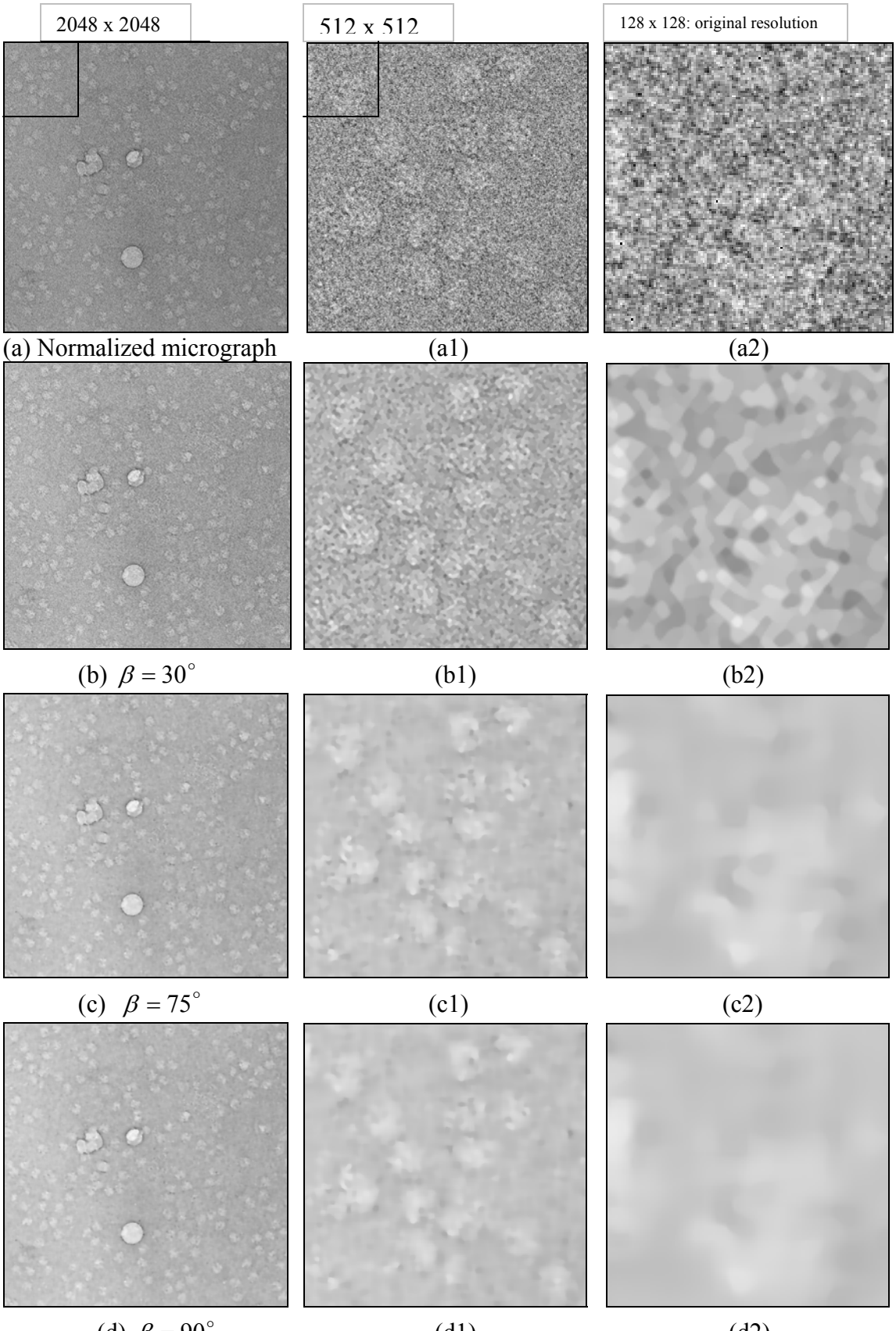

Figure 3: Effect of changing β in Beltrami-flow based smoothing.

values than the background, we replace each pixel grey level by the maximum in its neighborhood. The resulting image is an approximate representation of the background. In the second step, the background image is subtracted from the micrograph, and the grey values below zero are clipped to zero value. Figure 4, shows the result of pre-processing a histogram-stretched micrograph, after non-linear smoothing and rank-leveling.

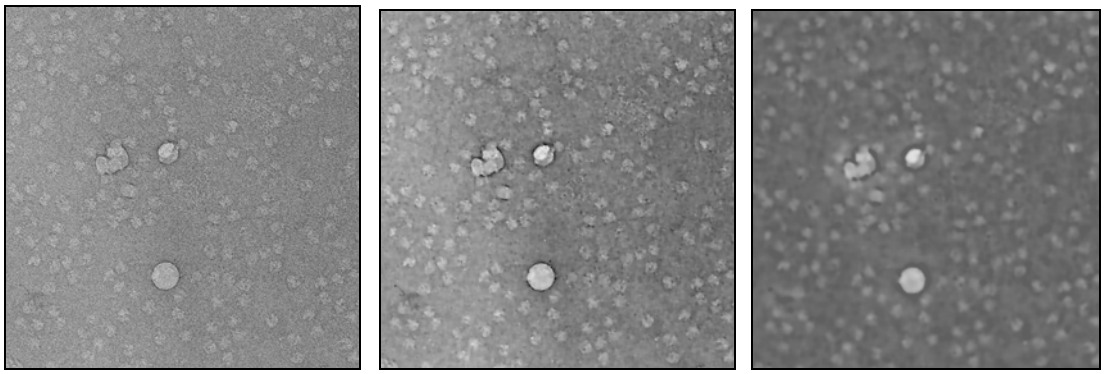

(a) (b) (c)

Figure 4: Result of pre-processing (a) histogram stretched micrograph, (b) after non-linear smoothing (c) after rank-leveling.

2.4 Segmentation of Particles

Ideally, a segmentation method finds those sets of pixels that correspond to distinct structures or regions of interest in the image and gives a unique label to each individual set. Segmentation of complex images involves several stages such as thresholding to separate background from foreground, distinguishing artifacts from objects, edge and/or region based algorithms to separate objects which are touching or closely located, component labeling and tuning the boundary pixel location for better precision.

2.31 Thresholding

Thresholding is a conversion from a grey-level image to a bi-level image. A bi-level image should contain all the information concerning the number, position and structure of the objects that are present in the grey-level image while containing much less other information. The problem is to select a proper threshold that accomplishes the above task. We have observed that selection of a single threshold for an entire micrograph is not possible in most of the cases due to overlapping of the grey-levels of the particles and background from different regions of the image. The first issue that must then be addressed, if regional thresholds are to be used, is to determine how many thresholds are needed and what the sizes of the regions are. We have implemented an adaptive region selection method. In the first step, the image is amplitude thresholded at a global mean intensity value $(k \cdot \mu)$ where k is a tuning parameter and μ is the mean intensity of the preprocessed micrograph. All connected components in the foreground are identified by component labeling (Dillencourt et al, 1992). Each such connected component is then considered as an individual region. In the second step, the mean grey level μ_i of connected component i is calculated. Connected component i is further thresholded at a unique threshold value ($k_1 \cdot \mu_i$). The tuning factor k_1 is experimentally set (we have used k=1.0 *and* k_1 = 0.5).

Bi-level micrographs thus obtained still contain many artifacts in the form of tiny isolated structures and small holes within the particles which are dealt with in the following way. Using a circular structuring element (Serra, 1982), the thresholded micrograph is 'opened'. If S is the structuring element and A is the image then grey scale opening of A by S is defined as $S \oplus \{S \Theta A\}$; where,

$S\Theta A = \min\{A[i-r, j-c] - S[r,c] | i-r, j-c] \in A[r,c] \in S\}$
$S \oplus A = \max\{A[i-r, j-c] + S[r,c] | i-r, j-c] \in A[r,c] \in S\}$; $\oplus$ is the dilation operator and Θ is the erosion operator. This opening operation reduces small noisy objects that resulted from thresholding micrographs that are still somewhat textured. Following this, a closing operation $S\Theta\{S \oplus A\}$, reduces noisy holes in the particles. The structural smoothing due to morphological filtering also force the objects to have a convex shape that can be better segmented. Figure 5 shows the result of multi-level, region-based thresholding followed by morphological opening and closing.

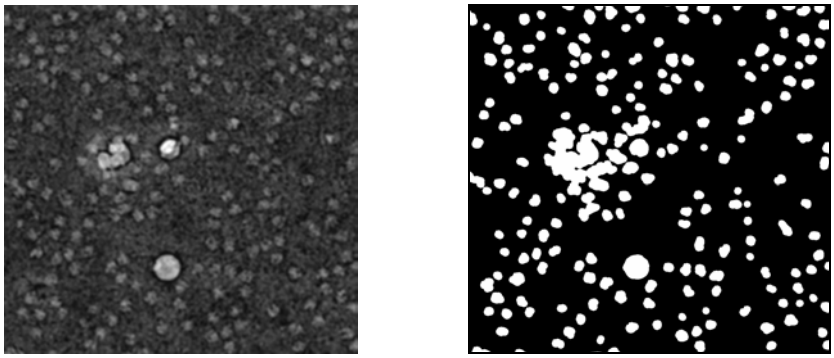

(a) (b)

Figure 5: (a) Part of the pre-processed image. (b) After thresholding and noise removal by morphological filters.

2.32 Relative Feature Filtering

Once the binarization process described above has been completed, it is still necessary to distinguish artifacts from individual particles and/or clusters of particles in the image. The use of some simple and intuitively obvious filters such as relative size and the relative average intensity of pixels within the candidate particle are recommended for this purpose. When the size and the average intensity values of the particles in the micrograph are known, this information can be provided as *a priori* information to the filtering process for selecting individual isolated particles and flagging cluster of particles for

further processing. Otherwise a data-driven process to filter-out the artifacts is recommended. We have tested one such approach in which the relative size of the object r_v is defined as the ratio of the size of that object to the average size of objects in the image. If the average size of the object i is $\overline{V_i}$, then

$$r_{v_i} = \frac{\overline{V_i}}{\frac{1}{\beta} \cdot \sum_{i=1}^{\beta} \overline{V_i}} \qquad \text{---------- (6)}$$

where β is the number of isolated objects present in the image. The relative intensity of the object r_{I_i} is defined as the ratio of the average intensity of the object pixels to the average intensity of foreground pixels in the image. If the average intensity of the object i is $\overline{I_i}$, then

$$r_{I_i} = \frac{\overline{I_i}}{\frac{1}{N_f} \cdot \sum_{k=1}^{N_f} I_k} \qquad \text{---------- (7)}$$

where N_f is the number of foreground pixels in the image. Particles are first ordered based on their sizes i.e. number of pixels within the particles. The average size is calculated by an α -trimmed filter which excludes α number of extreme size elements in the size ordered list of objects for calculation of the average object size $\overline{V_i}$ in the image (Oten, 2000). We have excluded 25% of the particles on both extremes of the ordered list of particles. All those particles with relative average-intensity less than 0.3 or relative size less than 0.5 are considered as artifacts and eliminated. Figure 6(a) is a normalized micrograph, Figure 6(b), shows a thresholded image while Figure 6(c) displays all the

isolated individual ribosome particles. In addition, objects with relative mean object size more than 1.5 are considered as possible clusters of particles and are flagged off for further segmentation. Figure 6(d) shows the image that has been flagged-off for further segmentation which we call the “residue image”.

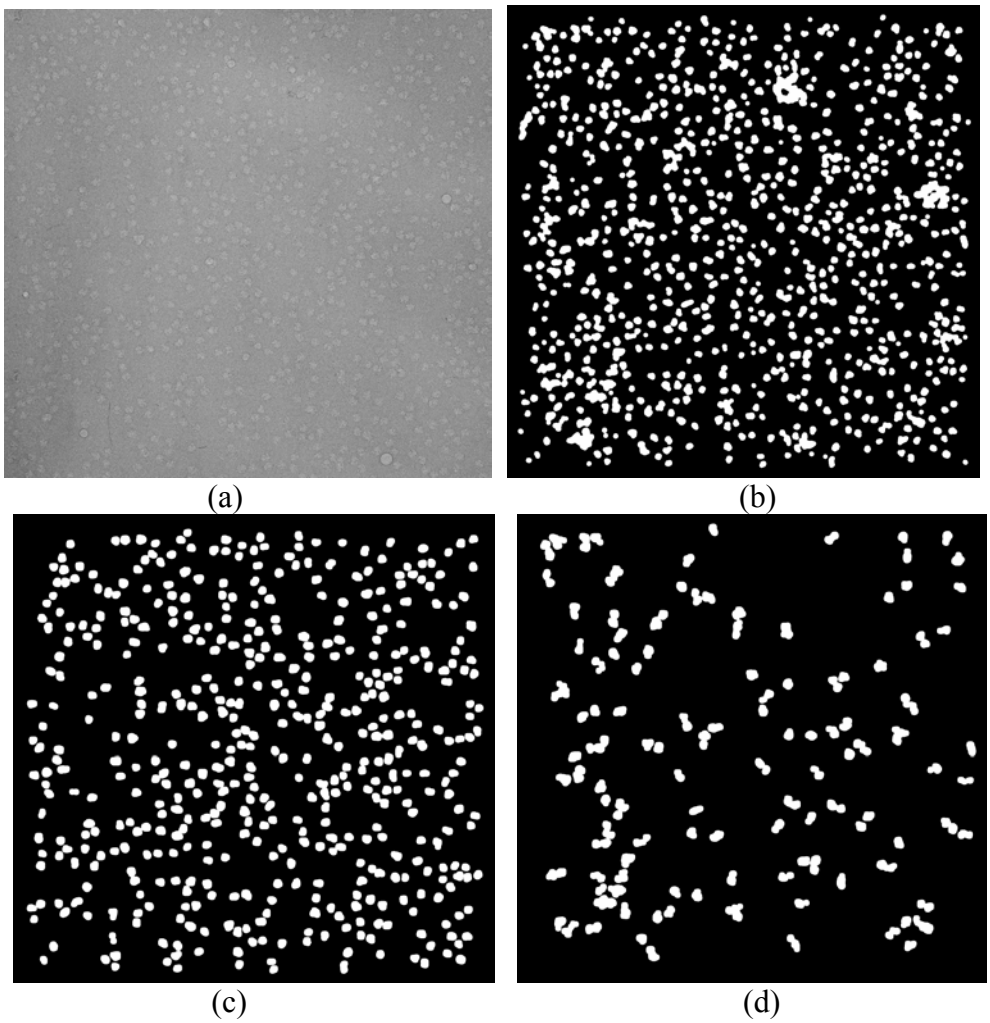

Figure 6: (a) Normalized micrograph (b) After binarization (c) Objects isolated as individual particles (d) Objects flagged off as cluster of particles. Note that the larger white “clumps” in (b) have been eliminated from (c) and (d) by relative size filtering.

2.33 Cluster Segmentation

The residue-image, consisting of particle clusters flagged off by relative feature filtering, is labeled using a component labeling algorithm. Segmentation of clusters is done in two independent stages.

Stage 1: The foreground of the residue-image is eroded one pixel thickness at a time. Ideally, this erosion process continues until a unique marker is obtained for each particle in the region of interest. Markers are the small group of connected pixels located at the approximate center of individual particles. The markers are tagged with a unique label and the number of erosion iterations needed to bring it to marker size. In the second step, markers are subject to controlled dilation. Markers are grown into their neighboring background pixels under certain conditions.

- No two growing markers are allowed to overlap or touch one another.
- The growing process is terminated when the grown region covers all the foreground pixels in the original residue-image.

A pixel level logical AND operation between the residue image and the dilated markers image provides segmentation of many particles in the cluster. The relative size filter with feature parameters obtained from already isolated particles can then be used to extract particles that are isolated by the erosion-dilation process.

Stage 2: If there are clusters of particles still left in the residue-image, then a final step of segmentation based on region growing over a distance map, which is a generalized version of the watershed technique, is applied (Vincent and Soille, 1991; Adiga and Chaudhuri, 2001). A distance map of the residue-image is generated using the Borgefors algorithm (Borgefors, 1996). Homogeneous regions in the distance map are identified

and the distance values of those pixels are rescaled to reduce flat fields (Bleu and Joshua, 2000).

Let *dist(.)* represent the distance value of pixels in the distance map.

Step 1: Connected group of pixels having maximum distance $d_{\max}$ in the distance map are considered as markers. A marker may consist of single pixel or a group of connected pixels. The markers are labelled by the component labelling algorithm. Let $d_{\max}$ be the maximum distance in the distance map, d_{next} is the next maximum distance level and $d_{\min}$ is the minimum distance value in the distance map.

Step 2: Pixels having a distance value (d_{next}) and located in the immediate neighbourhood of the labelled regional markers are merged with their neighbouring regional marker. This step can also be viewed as growing markers into their neighbourhood pixels that have a distance value d_{next} by reassigning their distance values to be $d_{\max}$ and tagging them with the corresponding label of the marker.

The isolated pixel or group of connected pixels in the distance map with distance d_{next} and not having a labelled regional marker in their immediate neighbourhood are considered as new markers and given a new unique label as well as having its distance value upgraded to $d_{\max}$.

Step 3: d_{next} = next maximum distance value in the image which is less than $d_{\max}$

Step 4: If the $d_{next} \neq d_{\min}$ then steps 2 and 3 are repeated.

The resulting image is filtered using relative size filters. Figure 7, shows an example of segmentation of clusters of ribosome particles.

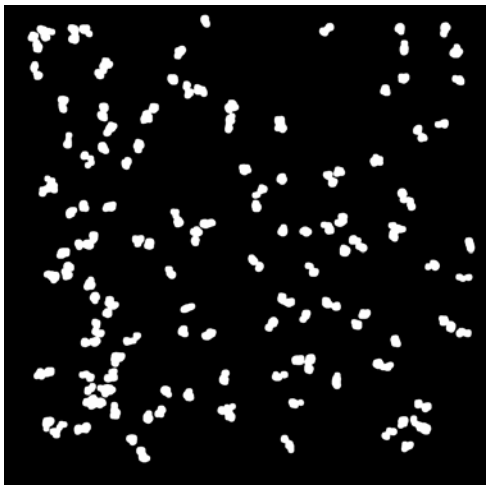

(a)

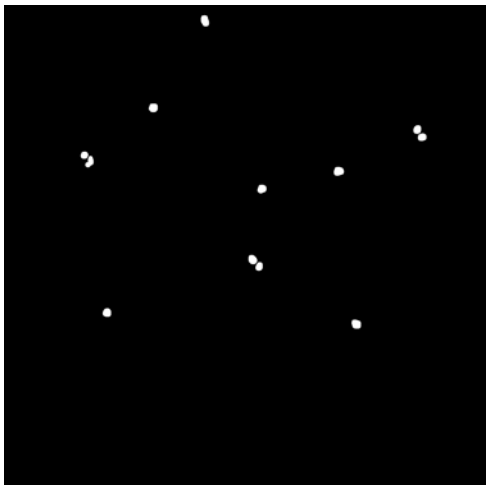

(b)

(c)

Figure 7: (a) Same as Figure 6(c),
(b): Result of erosion-dilation,
(c) Result of region growing / watershed on a distance map for segmenting clusters

A second stage of analysis is necessary to identify missed ribosome particles in the first stage. Every segmented particle projection in the original unprocessed micrograph is replaced by a background texture patch. The resulting image is then considered as a new, pre-processed micrograph, and all the steps of segmentation are applied again. As most of the parameters controlling segmentation are data driven, it is not necessary to retune them at this intermediate stage. Particles thus extracted are added to the original set of segmented particles. Figure 8 shows the result of second stage analysis to pick particles that were left-out in the first stage. We have observed that about 10-to-15% of the total particles segmented are obtained from the second stage of

processing. The increase in number of false positives due to the second stage of processing is negligible.

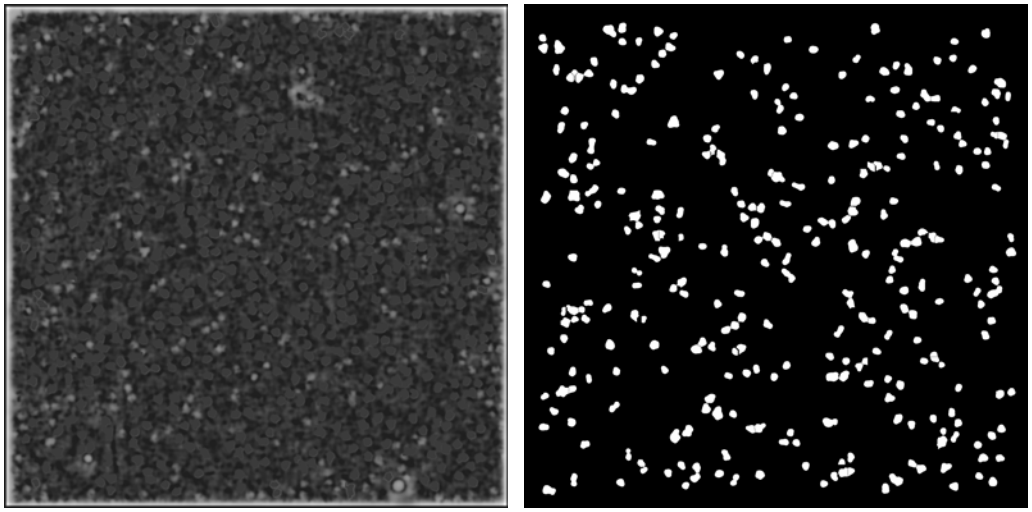

(a) (b)

Figure 8: Illustration of second stage of particle picking (a) Pre-processed micrograph after replacing all the particle area by a grey value less than the mean grey value of the pre-processed micrograph, (b) Particles and particle clusters picked during the second stage only.

Our aim is to extract each particle as a small sub-image. All the sub-images should have the same size (same number of columns and rows) so that they can be used for further analysis towards 3-D construction. To accomplish this, the centroid of each particle that is segmented from the micrograph is calculated, and a fixed size box is stamped around the centroid such that the complete particle is enclosed within the box. Figure 9 shows an example of a micrograph where segmented ribosome particles are boxed.

3. Experimental Results and Discussion:

The basic idea behind this methodology for picking ribosome particles is to pre-process the image to an extent that the standard segmentation algorithms can successfully identify each particle in the image.

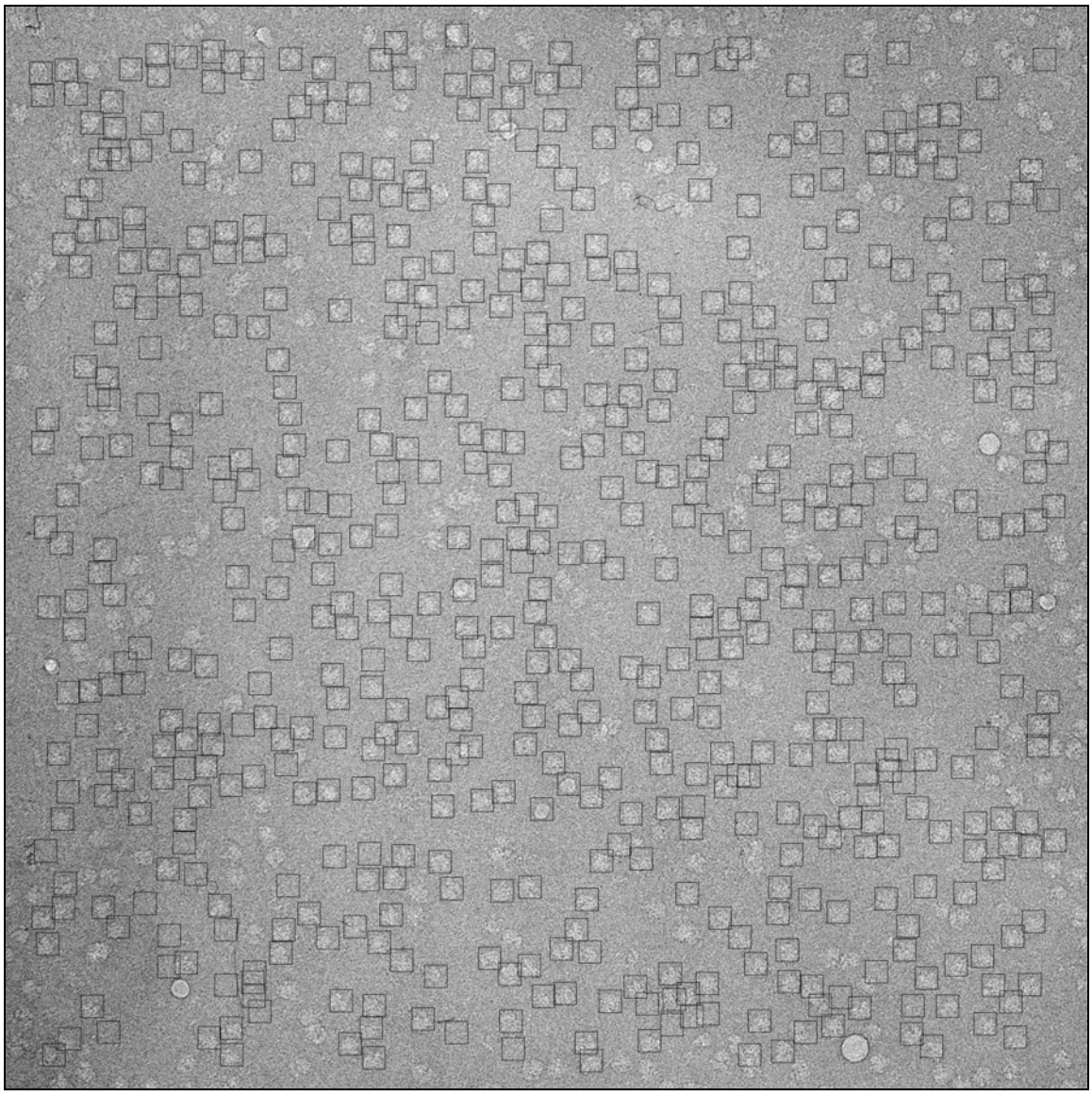

Figure 9: Illustration of boxing of recognized ribosome particles. Most of the apparent ribosome particles that can still be seen without boxes are, in fact, particles that are not picked by human either.

A two tone version of the image is then used to measure the size (i.e. the area) of the particles and the average density within this area is further used to identify the particles. Our goal is to consistently achieve, on a large set of data, 80% efficiency with respect to manual selection, with less than 10% false positives contained in the data set, and to do so without human intervention.

Table 1 gives a quantitative analysis of the efficiency of our automatic procedure in the case of a few micrographs with routine image quality. We have achieved and in most cases exceeded the expected target of 80% recognition with less than 10% false positives. The efficacy of our approach needs to be further tested on a large number of micrographs before accepting the software as a routine tool for picking ribosome particles.

No.	Image Name	No. of Particles Manual	No. of particles Automatic	False Positives	Estimated False positives	% recognition/ efficiency
1	Smic01	591	583	25	11	94%
2	Smic02	645	596	21	8	89%
3	Smic03	634	521	18	14	80%

Table 1: Quantitative analysis of manual particle picking and automatic method

The image files Smic01.spi, Smic02.spi and Smic03.spi, with particle coordinates that are known from manual boxing, were used as gold standards to test the performance of the protocol and to establish the parameter values used in the algorithm. The number of particles that were boxed both manually and automatically was used to compute the efficiency of the software with respect to the manual boxing process. If

$\Theta_{man} = \{p_1, p_2, ..., p_n\}$ is the set of manually boxed particles, where the size of the set $\#\{\Theta_{man}\} = n$, and $\Theta_{aut} = \{p_1, p_2, ..., p_m\}$ is the set of particles boxed automatically, where $\#\{\Theta_{aut}\} = m$, then $\{\Theta_{man} \cap \Theta_{aut}\}$ is the set of particles that are picked by both automatic and manual methods. The symbol '$\cap$' is the set intersection that brings out those elements that are common to both sets. The set $\{\Theta_{man} \setminus \{\Theta_{man} \cap \Theta_{aut}\}\}$ is the set of particles that are manually picked but not picked up by the software. The symbol '\' denotes the set difference. The set, $\{\Theta_{aut} \setminus \{\Theta_{man} \cap \Theta_{aut}\}\}$ is the set of false positives i.e. set of particles boxed by the automatic method while rejected as non-particles by the manual method. The percentage efficiency of the automatic method is then calculated by $\%\ efficiency = \frac{\#\{\Theta_{man} \cap \Theta_{aut}\}}{n} \times 100$. The particles that are marked by the automatic process but not by manual boxing are considered to be false positives. The efficiency of automatic particle picking, as defined above, is calculated based on the total number of false positives listed in column 5 rather than the estimated number listed in column 6 of Table 1. The column "estimated false positives" is provided because some of the boxes that are marked by the software, but not by the manual process, appeared to have actual particles in them.

Increasing β increases the diffusive property of the anisotropic diffusion process. An optimal trade off between protecting the boundary of the particles, and smoothing the noisy texture in the interior of the particles as well as in the image background, is achieved by trial-and-error. This trade-off resulted in our choice of $\beta = 75^\circ$ as a default value, as it produced a marked reduction in the already small percentage of false positives

with only a modest loss in the recognition of true positives. Table 2 shows the effect of using different values of β in the Beltrami flow based pre-processing.

Image. Name	Manual Pick	PDE $\beta = 30^\circ$ count / false +ve	PDE $\beta = 45^\circ$ count / false +ve	PDE $\beta = 62.3^\circ$ count / false +ve	PDE $\beta = 75^\circ$ count / false +ve	PDE $\beta = 90^\circ$ count / false +ve
Smic01	591	533 / 71	589 / 64	646 / 57	583 / 25	484 / 28
Smic02	645	513 / 51	546 / 48	558 / 45	596 / 21	433 / 30
Smic03	634	598 / 81	580 / 58	601 / 47	521 / 18	455 / 31

Table 2: Effect of the smoothing parameter on particle picking

It has been observed that our software performs with a better computational efficiency when the images are of size, say, 1024 x 1024, rather than when they are 4096 x 4096 and above. This is an issue of implementation of the algorithms and the efficiency of the computer. To make our software work efficiently for a large image on smaller machines such as PC, etc., a divide and conquer method can be adopted. The large image is divided into optimum size for the software to run efficiently on each image part. When each image part is processed, however, we reject those particles that are too close to the image border. For example, when an image of 4096 x 4096 pixels is divided into sixteen parts of size 1024 x 1024, a large number of particles in each part would be rejected as being too close to the border. This problem can be solved by not rejecting any objects until the whole image is reconstructed by tiling individual, processed/segmented, image parts.

To complete all stages of automatic particle picking on a 2048x2048 image with about six hundred particles, the program took twenty-one minutes on a 1GHz / 256Mb PC with Win2000 operating system. The program is implemented in Interactive Data Language (www.rsi.com). Re-implementing it in C or C++ would improve the efficiency at least by 50%. The efficiency of the program is also directly related to the quality of the image and the number of single isolated particles present, as well as the number of particle clusters present.

An important difference from the existing methods of particle selection is that this method can be defined as blind, as no manual intervention is allowed. The high degree of accuracy achieved in particle selection is due to extensive pre-processing that improves the particle contrast from its background. The application of the PDE-based Beltrami flow equation for smoothing and enhancing features helps in retaining the particle boundary, which in turn preserves the particle size and shape. Though the program was tested on relatively similar data sets, we expect it to work generally well on all micrographs acquired with similar instrument settings. Under different settings, retuning of one or several parameters may be necessary.

Acknowledgement: We would like to thank Dr. Kenneth Downing, Dr. Eva Nogales and Dr. Joachim Frank for important discussions and advice. Dr. William Nicholson provided key support in earlier stages of the related work that lead up to the approach reported here. This work has been supported by the Director, Office of Science, US Department of Energy Contract No. DE-AC03-76SF00098; NIH grant GM62989; and a grant from the Agouron Foundation.

References

1. Alvarez L., Lions P.L., Morel J.M., 1992. Image selective smoothing and edge detection by non-linear diffusion (II). SIAM J. of Numerical Analysis, 29, 845-866.
2. Bleu A., Joshua L.L., 2000. Watershed based Segmentation and Region Merging, Computer Vision and Image Understanding, 77, 317-370.
3. Borgefors G., 1996. On digital distance transforms in three dimensions, Computer Vision Graphics and Image Processing, 64, 368-376.
4. Catte F., Lions P.L., Morel J.M., Coll T., 1992. Image selective smoothing and edge detection by non-linear diffusion, SIAM J. Numerical Analysis, 29,182-193.
5. Dillencourt M.B., Samet H., and Tamminen M, 1992. Corrigenda: A general approach to connected component labeling for arbitrary image representations, *Journal of the ACM*, 39, 985-986.
6. Frank J., 1996. Three-dimensional Electron Microscopy of Macro-molecular Assemblies, Academic Press, San Diego.
7. Glaeser R.M., 1971. Limitations to significant information in biological electron microscopy as a result of radiation damage. J. Ultrastruc. Res., 36, 466-482.
8. Henderson R., 1995, The potential and limitations of neutrons, electrons and X-rays for atomic resolution microscopy of unstained biological molecules. Q. Rev. Biophys., 28, 171-193.
9. Jin J.S., Wang Y., Hiller J., 2000, An adaptive non-linear diffusion algorithm for filtering medical images, IEEE Trans. on Information Technology in Biomedicine, 4, 298-305.

10. Lata K.R., Penczek P., Frank J., 1995. Automatic particle picking from electron micrographs, Ultramicroscopy, 58, 381-391.
11. Malladi R., and Ravve I., 2002. Fast difference schemes for edge enhancing Beltrami flow, in: Heyden et al. (Ed.), Computer Vision ECCV 2002, Vol. LNCS 2350, pp. 343-357.
12. Malladi R., Ravve I., 2001. Fast difference scheme for anisotropic Beltrami smoothing and Edge contrast enhancement of Gray level and Color images. LBNL Tech Report-48796, Lawrence Berkeley National Laboratory, University of California, Berkeley.
13. Malladi R., I. Ravve, 2001. Fast difference scheme for anisotropic Beltrami smoothing and Edge contrast enhancement of Gray level and Color images. LBNL Tech Report-48796, Lawrence Berkeley National Laboratory, University of California, Berkeley.
14. Malladi R., Sethian J. A., 1996. Image Processing: Flown under min/max curvature flow and mean curvature, Graphical Models and Image Processing, 58, 127--141.
15. Nicholson W.V., and Glaeser R.M., 2001. Review: Automatic Particle Detection in Electron Microscopy, J. Struct. Biol., 133, 90-101.
16. Nitzberg M., Shiota T., 1992. Nonlinear image filtering with edge and corner enhancement, IEEE Trans. on Pattern Analysis and Machine Intelligence, 14, 826:833.
17. Osher S., Sethian J.A., 1988. Fronts propagating with curvature dependent speed: Algorithms based on Hamilton-Jacobi formulations, J. Comput. Phys., 79, 12-49.

18. Oten R., 2000. Nonlinear Signal and Image Processing based on Order Statistics, Ph.D. Thesis, University of California, Irvine.
19. Perona P., Malik J., 1990. Scale space and edge detection using anisotropic diffusion, IEEE Trans on Pattern Analysis and Machine Intelligence, 12, 629-639.
20. Polyakov A.M., 1981. Quantum geometry of bosonic strings, Physics Letters B, 103B(3), 207-210.
21. Rudin L., Osher S., Fatemi E., 1992. Nonlinear total variation based noise removal algorithms, Physica D, 60, 259-268.
22. Russ J.C., 1995. The Image Processing Handbook, CRC Press, London.
23. Sali A., Glaeser R.M., Earnest T., and Baumeister W., 2003. From words to literature in structural proteomics, Nature, 422, 216-225.
24. Serra J., 1982. Image Analysis and Mathematical Morphology, Academic Press.
25. Sochen N., Kimmel R., Malladi R., 1998. From high energy physics to low level vision, LBNL report #39243, Lawrence Berkeley National Laboratory, University of California, Berkeley, USA.
26. N. Sochen, R. Kimmel, R. Malladi, 1998. A general framework for low level vision, IEEE Transactions on Image Processing, special issue on PDEs and Geometry-Driven Diffusion in Image Processing and Analysis, 7, 310—318.
27. Umesh Adiga P.S., Chaudhuri B.B., 2001. An efficient method based on watershed and rule based merging for segmentation of 3-D histo-pathological images, Pattern Recognition, 34, 1449-1458.

28. Vincent L., Soille P., 1991. Watersheds in digital spaces: An efficient algorithm based on immersion simulations, IEEE Transactions on Pattern Analysis and Machine Intelligence, 13, 583-593.